The Korean Journal of Ceramics, **5** [1] 55 - 72 (1999)

Tailoring and Control of The Micro (Nano) Structure of Functional CMC's and MMC's

Colomban[a,b]

[a]*Laboratory for Dynamics, Interactions and Reactivity, Centre National de la Recherche Scientifique UPR 1580-CNRS, 2, rue Henri Dunant 94320 Thiais, France and*
[b]*Materials and Composite Systems Department, Office National d'Etudes et Recherches Aérospatiales (ONERA) BP 72 93322 Chatillon, France*
(Received September 23, 1998)

A challenge in the aerospace field is to design new composites satisfying specific and sometimes conflicting properties. The key steps are i) the understanding and the control of the reaction between the reinforcement and the embedding matrix, ii) the achievement of a coherent and robust matrix. The problems encountered to prepare particulate, 1D, 2D and 3D reinforced composites using polymeric precursors are discussed. Emphasis is given to the control of the micro/nanostructure using Raman microspectrometry and depth-sensing microindentation, in order to get information on the micromechanics and fiber structure simultaneously, within ceramic (CMC's) and metal matrix (MMC's) composites.

Key words : Composites, Sol-Gel, Fibres, Micromechanics, Raman

I. Introduction

One of the key steps in the advancement of the materials processing is the achievement of a special and controlled microstructure, in order to satisfy specific and sometimes conflicting properties, preferably using low cost methods. This is particularly true for composites. The great weakness of monolithic ceramics (and to some extent of intermetallic superalloys), due to their polycrystalline state and the nature of the chemical bonds existing in these compounds, is their intrinsic inability to tolerate mechanical damage without brittle rupture. The addition of a particulate reinforcement or, better, the incorporation of long ceramic fibers, results in a metastable material -a composite-exhibiting greater toughness with pseudo-plastic characteristics.[1] These composites would be promising materials for thermostructural applications if this metastable state could be preserved during the synthesis, and then in the working atmosphere, without internal corrosion of the fiber by the matrix and vice-versa.[2,3]

To date high strength and high toughness C(SiC) fiber/ C(SiC) matrix composites are produced by Chemical Vapor Infiltration (CVI).[4,5] They are very expensive since the specific tools which maintain the fiber during the process, in order to achieve a coherent and rather dense matrix, are not reusable. Infiltration can be achieved only by gaseous (CVI method) or liquid precursors for which the ceramic yield is necessarily low, which implies porosity and cracks after firing or a very slow multisequenced process. The matrix precursor must be introduced between fiber yarns (a few micron or less in spacing) through interyarn voids of a few millimeters. Fig. 1 shows an example of interyarn voids filled by an alumina matrix. The presence of a fiber preform with invariable geometry always inhibits the coherent shrinkage of the matrix, the addition of "inert" reinforcements being detrimental to the densification. Even the homogeneous dispersion of anisotropic particles in a powder and the compaction of the resulting mixture become difficult to achieve when the content of added particulate reinforce-

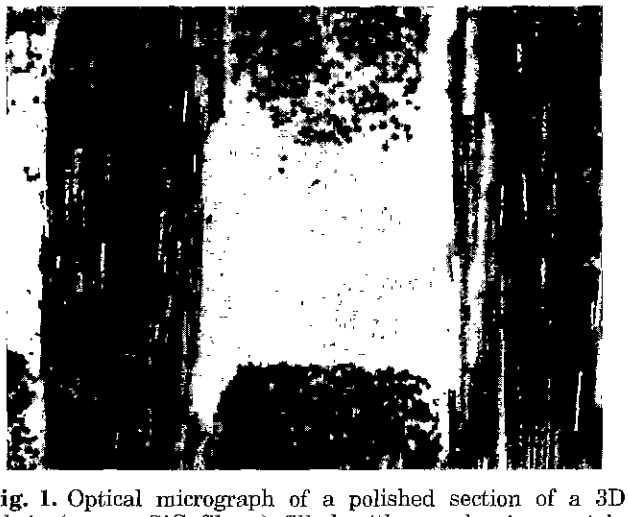

Fig. 1. Optical micrograph of a polished section of a 3D fabric (woven SiC fibers) filled with an alumina matrix (fiber diameter ~14 μm).

ments (whiskers, platelets, short fibers) reaches values (ca. 10-30%) increasing the toughness significantly.

The objective of this review is to show that the use of polymeric precursors constitutes a unique tool for the processing of multiphase materials with tailored micro- and nanostructure thanks to the unusual characteristic of gels and polymeric precursors, for instance the viscosity, the gelation, the meso/microporosity, the easy nucleation of one phase from a pristine amorphous state, etc. The above requirements need special processing and control techniques. Because interactions between processing parameters make optimization a complex process, micro and nanostructure control is mandatory. The examples discussed hereafter are chosen both in the open literature and among the works conducted at the Office National d'Etudes et de Recherches Aerospatiales (ONERA, French National Establishment for Aerospatice Research) in order to give a complete view of the methods based on polymeric precursors. We will show that Raman microspectrometry and depth-sensing microindentation are well-suited methods to provide simultaneously informations on the physical-chemical state of the phases and on the compressive/tensile strain applied to a fiber/particle embedded in a matrix. Examples are chosen among (SiC, C) fibers/platelets reinforced (mullite, Nasicon, TiAl superalloy) matrix composites.

II. Experimental Procedure

1. Sample Preparation

The preparation of particulate, two-dimensional and three-dimensional fiber reinforced composites will be presented briefly with the discussion of the nano- and microstructure tailoring methods. Details have been previously reported (see Table 1).[6-39] Matrices were prepared using commercially available submicronic powders or powders especially prepared by hydrolysis of various alkoxides mixtures and subsequent thermal treatment. Commercially available polyvinylsilane and alkoxides were also used to fill a fiber preform already filled with a submicronic powder. Tailored alkoxide mixtures were used as interface precursors to control the fiber-matrix reaction and to enhance the matrix sintering.[7-14]

2. Techniques

Raman spectra were recorded with the 514.5 nm exciting radiation of an argon ion laser, using a Dilor XY spectrograph equipped with a double monochromator as a filter, and a liquid nitrogen-cooled Wright CCD mosaic detector. The laser beam was focused in air at normal incidence on a small area of the fiber/the matrix (ca. 1 μm^2), using a microscope. The total magnification was 1000 and the backscattered light was collected with the microscope. Spectral line scans and mappings were recorded with the 632.8 nm exciting line of a krypton ion laser, using a "System 1000" Renishaw spectrograph equipped with a 200K cooled CCD mosaic detector. The great precision we needed for the processing of the spectra made it a requirement to use laser plasma lines or to introduce a Neon lamp in the spectrograph chamber to serve as a wavenumber absolute reference. It was also mandatory to check that the wavenumber heating shift provoked by the laser beam induced sample heating remained lower than 1 cm^{-1} and was reproducible. Finally, the peaks fitting along their whole extent, was performed using the 4 version of the Microcal Origin peak-fitting software (by Microcal Solftware Inc.). Details can be found in refs.[15-16]

The relationship linking the Raman wavenumber shift of carbon-containing fibers to the tensile strain was calibrated as described in ref.[16] The fibers used for this purpose have been annealed to reproduce the conditions of preparation of the CMC's for the characterization of which calibrations would be called for.[17]

Local Young's modulus (E), Vickers, microhardness (Hv) and interfacial frictional shear stress (τ) were determined using a home-made Vickers depth-sensing microindenter.[18] The load cell measures load up to 1N with an accuracy of about 0.5 mN. The displacement gauge has an accuracy of a few nanometers. The loading rate is

Table 1. CMC's Prepared using Polymeric Precursors

Reinforcement	Matrix	Function	Specific Properties	References
Particles	Resin Glass	Cutting tools	Abrasive	28,31
Mica	Ceramics "	Structural parts Machinable parts	High toughness Machining	12 32
1D (and 2D cross-ply)	Aluminosilicates	Thermostructural parts	High strength Damage tolerant	33-39
2D (textile)	Mullite Celsian SiC	Thermostructural parts " "	High strength Damage tolerant	6,7,9,10,27
2D 2.5D	Nasicon Mullite	Thermostructural Microwave absorbing parts	Tailored ε/σ Damage tolerant	8
	SiC	"	"	27
3D (textile)	Alumina SiC	Thermostructural part	Damage tolerant	11 27

load-controlled and varies from 5 to 30 mN/s. The position of the indenter with respect to the polished surface of the sample and the applied load are measured continuously during testing. This enables the hardness and Young's modulus to be determined without the need for direct imaging of the indentation. However, the size and shape of the indentation were always checked using the method described in ref.[18]

III. Results and Discussion

1. Processing

1.1. Liquid Ceramic Precursors Based Methods

The use of synthetic liquid ceramic precursors takes inspiration in the "old" whiteware technology based on the natural colloids properties which makes it possible to achieve enamel coating, shape forming, cold molding, porosity control and use, etc.[19] The idea of using polymeric ceramic precursors for the consolidation of a fiber preform originates from the processing route used for C/C composites: infiltration by pitch or phenolic resines. The main parameters to be controlled are the viscosity, the achievement of a dense green body, which can be related to wetting control, the *in situ* gelation, to make it possible to keep the precursor inside the preform, the yield of the precursor-to-ceramic conversion, the composition and the state (amorphous, crystalline, porous, etc.) of the pyrolyzed materials.[19-24] The importance of each parameter depends on the nature of the reinforcements (particles, 1-dimensional fibers, 2D woven fibers (textile) and 3D textile or fiber preform) and on the matrix composition.

1.1.1 Oxide Precursors

Gelation of liquid oxide precursors, alkoxides (M(OR)n) for instance, results from hydrolysis-polycondensation :

$$M(OR)_n+nH_2O \rightarrow M(OH)_n+nROH,$$

and simultaneously, generally, $M(OH)_n \rightarrow n/2H_2O+nMO_{n/2}$.[19,20]

In fact, after drying the resultant gel has a complex composition such as $MO_{n-x-\varepsilon}(OH)_{2x}(O\text{-}R)_{2\varepsilon}mH_2O$ with x~0.1-0.3, m=3-6 and $\varepsilon \leq (0.01$.[21] Oxide gels are made of polymeric entities (diameter 0.5-2nm), which are more or less densely packed according to the hydrolysis-polycondensation rate and the initial alkoxide-to-solvent and alkoxide-to-water ratios.[22] The gel is converted into a meso/microporous xerogel also called "porous glass" by thermal treatment above ca. 300°C. The shrinkage related to the gel densification is suppressed. Consequently, the gel plasticity disappears. The presence of some M-OH "dangling" bonds in place of M-O-M bridges stabilizes the surface of the porous network which makes the densification sensitive to the atmosphere (H_2, vacuum, air).[23] Densification and nucleation for refractory or glass-reluctant compositions result from the short range structural rearrangement induced by surface dehydroxylation at about 0.5 Tm (Tm: melting temperature).[23,24] It can be compared to the 0.8 Tm value usually required for the sintering of a fine ceramic powder. There is thus a relationship between the hydroxyl content, the composition and the meso/microporosity of a (xero)gel. The nanostructure can therefore be tailored by the chemical parameters controlling the inorganic polymerization and the hydroxyl content (relative proportions of reagents, addition of complexing liquids, temperature, sonification, sintering atmosphere, etc.[20-22] In the case of glass-forming compositions, a viscous sintering may occur while the dehydroxylation-densification proceeds.[19,20] In this case, bloating can be observed if gas departure (H_2O from dehydroxylation, CO_2 from oxidation of unhydrolized organic branches) is hindered.[13] Among commercially available reagents we have selected, aluminium-s-butoxide $Al(OC_4H_9)_3$, tetraethoxysilane $Si(OC_2H_5)_4$, aluminum-silicon ester $(OC_4H_9)_2$-Al-O-$Si(OC_3H_9)_3$, zirconium i-propoxide $(Zr(OC_3H_7)_4$, tributylborate $(B\text{-}(OC_4H_9)_3)$ and tributylphosphate $(P\text{-}(OC_4H_9)_3)$. Home made germanium propoxide $Ge(OC_3H_7)_4$ was also used. The handling of aluminum and germanium alkoxides requires a glove box free of H_2O traces. The viscosity of the alkoxides can be adjusted at values 0.7 poise by heating below 80°C. One of the main interest of liquid alkoxides is that they exhibit a rather good ceramic yield: typically the alkoxide-to-ceramic conversion yield is comprised between 20 and 30wt%. Mixing of liquid precursors promotes the intimate combination of various precursors at the molecular scale and allows to adjust the viscosity to voids' filling requirements.

1.1.2. Covalent Matrix Precursors

Since the work of Yajima *et al.*,[25] polycarbosilane (PCS) is well-known as a precursor of SiC-based Nicalon fibers. However, the high viscosity of this precursor prevents its use to fill a fiber preform already filled with a submicronic powder. Furthermore, the oxygen driven reticulation of the chains of the precursor inside a thick sample is not obvious, which makes difficult the control of the stoichiometry in the whole part. At the ONERA, we have developped a polyvinylsilane (PVS) fulfilling the specific requirements for the infiltration of a porous body[26,27]: i) a thermostat behaviour with a cross-linking temperature (200-300°C) far enough of the begining of pyrolysis (400 °C) to avoid bubles formation during cycle, ii) a relatively low molecular weight (Mn<1000), in order to achieve a sufficiently low viscosity at room temperature (<10 poises), to allow injection in the fiber preform at a higher temperature (0.3 poise at 130°C) compatible with the gelation temperature, iii) a very high ceramic yield: 64% in weight and iv) a rather good Si/C stoichiometry to obtain air stable materials.[27]

1.2. Particulate Reinforced Composites

1.2.1. Abrasive Grains

Apart from the coating of a surface (plate, fiber -this topic will not be discussed in this review-), the most "simple" application of sol-gel materials is as abrasive grains. Abrasive particles can be dispersed into vitrified or resin bonded grinding wheels, coated abrasive belts,

sheets and discs. In 1981, 3M Company introduced the first sol-gel abrasive particle referred to Cubitron™ grain in the Regal™ coated abrasive fiber disc product line.[28] The idea to use sol-gel processing had originated from the processing route of ceramic fibers developped at 3M by Sowman[29] some years ago. Commercially available boehmite (AlOOH) sol, derived from the hydrolysis of aluminium alkoxide, a by-product of the Ziegler process for the production of long chain alcohols. A metal salt is added to the sol, gelation provokes and a stiff gel is formed. Afterwards, this gel is dried, crushed and screened to the appropriate size distribution, calcined and then sintered at a temperature between 1200 and 1600°C. The resulting material is screened and ready to be used as an abrasive particle.

Non-oxide ceramics are finding increasing applications as high-speed cutting tools for metals.[30] The combination of sol-gel processing and reaction-sintering has been used to prepare dense non-oxide abrasive grit.[31] An Al_2O_3 sol was prepared by dispersing boehmite powder into HNO_3 containing water heated at ~80°C. The sol was seeded with (Al_2O_3 crystallites. The abrasive grains were prepared from the dispersion of carbon black and TiO_2 in the seeded Al_2O_3 sol. Glycerol was added to prevent oxydation of the carbon black during calcination. The gel was dried, crushed, screened and calcined at 1000°C and then thermally heated at 1400°C and then at 1900°C under a flowing N_2 atmosphere, for the formation of TiN and AlN by carbothermal reduction. The final microstructure (AlN/TiN/AlON) is controlled by the amount of TiO_2 in the sol and by the C content. The strong advantage of sol-gel abrasive particles is the ability to introduce chemical changes which modify the alumina crystal structure and enable the optimisation of the grinding.[31]

1.2.2. Particulate reinforced Ceramic Matrix Composites

Particulate reinforcement is used to improve the toughness of small, shaped pieces or to facilitate the machining. The machinable sol-gel prepared mica-ceramic composite can be cut by conventional metallic saw[32] and is used as an insulating material for precision machines and as a substrate for electronic parts.

Platelet and whisker reinforcement is used to increase the toughness of monolithic ceramics. The homogenenous dispersion of anisotropic particles in a powder and the compaction of the resulting mixture is always difficult because the applied load decreases with the number of contact points. The use of liquid aids (colloid processing) counteracts this drawback, although imperfectly. Gel embedding offers a new route for the mixing of powders and particulate reinforcements thanks to the incorporation of a viscous substance, the reactivity of which can be tailored by composition design.[12] Cold molding makes it possible to prepare shaped and crack-free pieces. The process is the following: powder and particles are dispersed together in an anhydrous solvent (e.g. propanol) before the addition of alkoxides. After mixing, pH controlled water is poured on under vigorous mechanical stirring, which has to be maintained until a paste of thick consistency is obtained. The paste is then dried to give a flour-like powder. The powder is compacted and sintered in air at 1600°C or, alternatively, hot-pressed under primary vacuum at 1450°C. In the example given in ref.[12], the used powder is a submicronic α-alumina powder (AKP50, Sumitomo, Japan) or a micronic mullite powder (Baikalox 6944, Baikovsky, France) and particulate reinforcements are α-alumina single crystals platelets (Atochem, France). Zirconia and alumina precursors are used. A sketch of the mixture cold pressing is given on Fig. 2: during cold pressing, the viscous gel creeps to fill the interparticle voids. Gel embedding promotes an homogeneous load/pressure transfer and hence suppresses the densification hindrance induced by the platelet addition. Examination of the microstructure shows the homogeneous dispersion of the oxide second phase resulting from the gel pyrolysis (Fig. 2). For example, zirconia gel embedding of the mullite powder increases the microhardness by 30% and the toughness by 40%. The combination of zirconia gel embedding and platelets addition increases the KIC value to ~5MPa.$m^{1/2}$.[12]

1.3. 1D and 2D Fiber Reinforced Composites

One of the main problems in the preparation of ceramic

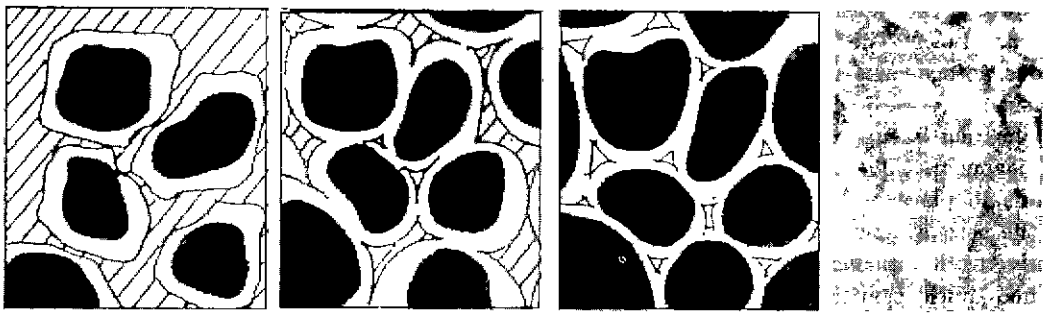

Fig. 2. *From left to right*: Sketch of the gel embedding (in white) and compaction of particulate reinforcements/grains (in black), porosity is dashed; after compaction, gel is squeezed between the hard particles. *Right*: Backscattered scanned electron photomicrograph of 1600°C sintered pellet, made of 30 wt% Al_2O_3 platelets in alumina matrix, gel embedding ZrO_2 precursor. (zirconia grains appear in white, mean size: 1 μm).

matrix composites is to achieve a low open porosity in the matrix, in order to protect the fiber from the environment and to optimize the mechanical strength and toughness. In the case of weavable fibers forming a yarn, the inter-fiber voids are a few micron or less in size, which makes infiltration of liquid or gaseous precursors mandatory, in spite of their low ceramic yield. In many cases, interyarn voids of textile preform are accessible only through inter-fiber voids (Fig. 1). C.V.I. methods based on the infiltration of gaseous precursors are expensive. Furthermore, gaseous precursors are not well suited for the multicomponent oxyde compositions required for functional composites.[10] The presence of a long fiber reinforcement, geometrically invariant, inhibits the coherent shrinkage of the matrix. In the case of 1D or 2D (textile) reinforcements, this phenomenon can be solved by hot-pressing: the in-plane shrinkage can be counterbalanced by the thickness reduction if a viscous behaviour is achieved during the hot-pressing.

Many attempts to prepare dense ceramic matrix composites by the sol-gel methods have been made. Many of them used mullite as the matrix material because of its excellent high temperature strength and creep resistance, good chemical and thermal stability, low thermal expansion coefficient and low permittivity. First, Qui and Pantano,[33] Pannhorst *et al.*[34] and then Russell-Floyd *et al.*[35] demonstrated that sol-gel processing can be used. Sheffield group[36-40] pointed out that highly densified unidimensional continuous carbon fiber reinforced mullite composites could be successfully prepared by a single stage infiltration process, using Ludox® colloidal silica sol (Dupont AS40) and α-alumina powder (A1000G, Alcoa), followed by hot-pressing. Briefly, the pH of the Ludox® sol was adjusted to 2-3 before dispersion of alumina powder.

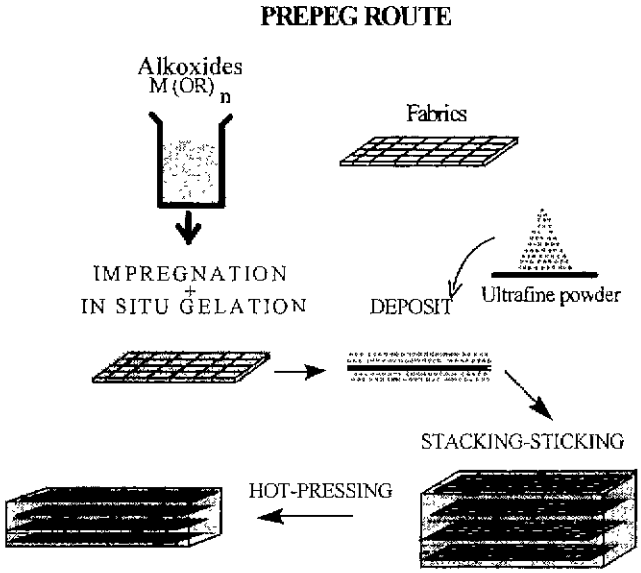

Fig. 3. Flow diagram of the sol-gel process for fabricating Functionaly Graded Ceramic Matrix Composites (FGCMC's) incorporating different fabrics and matrices. Ref.[13]

Composites reinforced with woven (C, SiC or oxyde) fibers could be successfully prepared by a two-step process,[8-10] illustrated in Fig. 3. First the fibers of a two-dimensional woven fabric are impregnated with a liquid alkoxide mixture (for instance for mullite matrix composite, a mixture of zirconium i-propoxide, aluminum-silicon ester, tributylborate and germanium propoxide), which fills the voids between the fibers, transforms into a gel, *in situ*, by reaction with atmospheric moisture and is to be converted into a (glass-) ceramic by pyrolysis during the hot-pressing step. Before pyrolysis, a fine, amorphous matrix precursor powder, suspended in chlorobenzene, is deposited onto the layers of woven fiber fabric (prepreg textile). This matrix precursor powder is prepared by rapid hydrolysis of the appropriate mixtures of alkoxides in propanol. The resulting gel is dried at ca. 750°C to drive most of the water and a part of the hydroxyl groups out and hence reduce the polymeric oxide network forthcoming shrinkage. Then, the doubly impregnated layers of textile fabric are stacked together in a graphite mold and hot-pressed between 1000 and 1400°C. Below 300°C, gel viscosity promotes homogenenous pressure application. A liquid sintering aid (for instance, B_2O_3 or GeO_2) obtained by pyrolysis of appropriate gel precursors can be incorporated.[6,9] Then, the liquid sintering aid is eliminated either by incorporation into the matrix or by volatilization. Therefore, it does not contribute to the formation of second phases at the grain boundary and does not decrease the thermal stability of the composite significantly.[10] The dwell temperature is related to the composition of the matrix and of the interphase precursor. The transitory liquid phase acts both to densify the matrix (sintering aid) and to maximize the contact between the grains of the matrix precursor during the hot-pressing step. Depending on both matrix and fiber materials, several different "interface precursors" can be used, either alone or in various combinations.

1.4. 3D Fiber Reinforced Composites: Near Net-Shape Sintering

For continuous 3D fiber reinforced bodies, the idea of using liquid ceramic precursors for the impregnation of the fibrous preform originates in the preparation of C/C composites by pitch or phenolic resin infiltration.[27] To mimic this route, the slip-casting of a submicronic powder has been proposed,[41] but this led to highly porous samples (open porosity close to 35-40%) exhibiting very poor mechanical properties and low protection of the fibers against corrosive atmospheres. Besides, the range between the consolidation temperature and the temperature at which the matrix shrinkage leads to a matrix cracking, within the geometric invariant preform or fabric, is small. Due to the fact that the achievement of a zero-porosity matrix is non-realistic for thermostable compositions, we will consider methods increasing the mechanical strength of a porous body. The first idea is to avoid cracks, maintaining a coherent matrix (maximization of the number

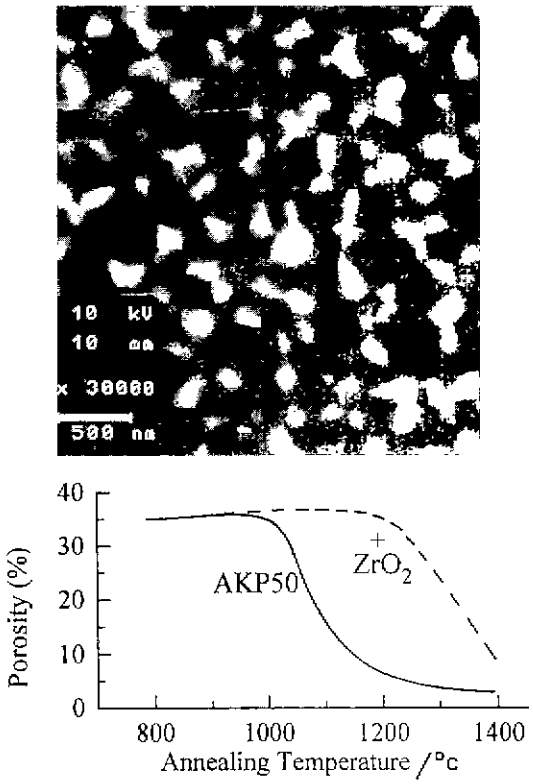

Fig. 4. Back scattered electron photomicrograph of the alumina matrix composite post-infiltrated with zirconia precursor, after thermal treatment at 1400°C. See the zirconia phase (in white) located between submicronic, round alumina grains. Comparison of porosity plots vs thermal treatment shows the +200°C shift of the sintering. Ref.[13]

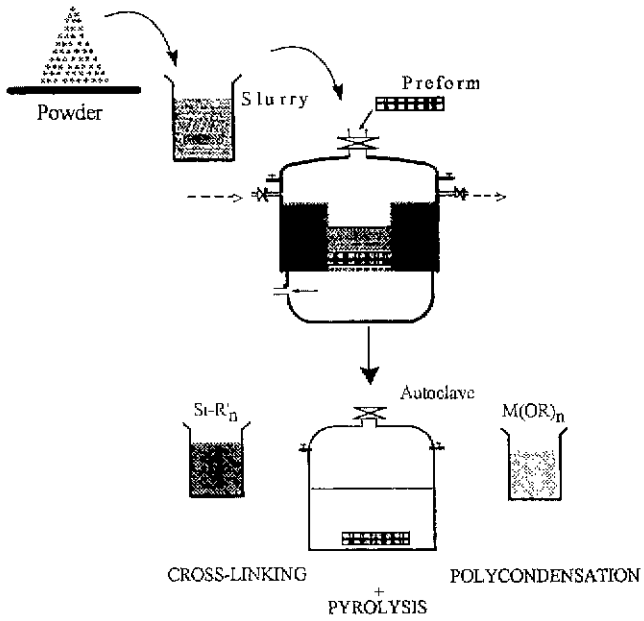

Fig. 5. Flow diagram of the "two-step" infiltration process for fabricating matrix near-net shape sintered CMC's. Alkoxides ($M(OR)_n$) or silicon derivatives ($Si\text{-}R'_n$) can be used Ref.[13]

of interparticulate bonds without shrinkage), the second one is to improve the strength of the interparticulate bonds and/or of the intergranular phase (maximization of the reaction between grains).

The first requirement can be obtained by filling the voids between slip-cast grains, with a ceramic precursor, which after a thermal treatment, is transformed into a refractory phase.[42] The resulting intergranular phase may form an inert barrier between slip-cast grains and thus put the shrinkage off to higher temperatures.[43] Fig. 4 gives an illustration of the post-infiltrated microstructure of the matrix used with a nearly isotropic carbon fiber preform (Noveltex from SEP, France) filled by a slurry of Sumitomo AKP50 alumina powder.[11] The mean size of AKP50 particle is 0.6 μm which allows to pass through interfiber voids. Thermal treatment at 1000°C was carried out in order to initiate the consolidation of the matrix without developping a significant shrinkage of alumina grains.

Fig. 5 shows a schematic of the two-step infiltration process.[11] The first step consists in the preparation of a powder compact within the fiber preform by a routine slip-cast infiltration, the body being dried and then strengthened by heating at a temperature close to the shrinkage onset. The second step consists in the infiltration of the strengthened body by a liquid (polymeric) precursor that is first converted into a solid (a gel by reaction with water or diols if alkoxides are used,[42] a resine by action of oxygen if polyvinysilane-PVS is used to prepare SiC matrix,[27] etc.) and then, during pyrolysis, into a refractory intergranular phase. This second step can be repeated as many times as necessary to optimize the interparticle bonding and to fill the porosiry.

Optimization of the microstructure might be involved by (i) the increase in ceramic yield of the precursor pyrolysis, (ii) the increase in thermostability of the resultant phase, in order to limit the shrinkage of the refractory interphase and postpone the whole matrix shrinkage towards higher temperatures, (iii) optimization of the fiber-matrix interface. For instance, various polymeric precursors can lead to inert, refractory and non-reacting interphases: Zr-i propoxide as zirconia precursor, Al butoxide as alumina precursor, Ln-alkoxide and homologues as rare-earth oxide precursor. Sometimes, Ti-i-propoxide as rutile precursor, tetraethoxysilane, as silica precursor, Al-Si ester as aluminosilicate precursor, ..., can be used. These last three compounds, which slightly react with many oxides, might also be used to strengthen the interparticle bonds (see below). It is however very important to keep, simultaneously, a net-shape sintering behaviour. Fozinstance, the room-temperature flexural strength was multiplied after five (Fig. 6) cycles of post-infiltration, in situ hydrolysis-polycondensation and 1000 °C heating, zirconium i-propoxide being used for the first four cycles and aluminium-silicon ester for the last one.[11,42] Measurements of the flexural strength at 1200°C or at 1300°C showed that the mechanical properties had increased by a factor 6.[11]

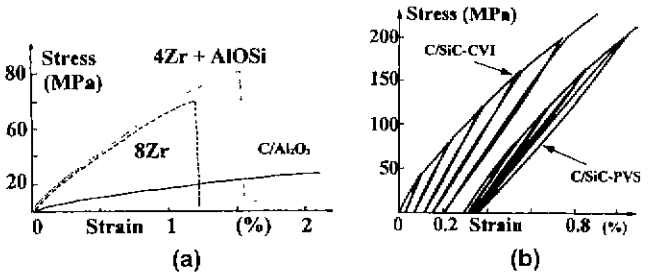

Fig. 6. a) Flexural stress-strain plot of a 3D Noveltex® carbon fiber preform-alumina matrix composite (C/Al_2O_3) and after, respectively, eight cycles of post-infiltration, 1000°C thermal treatment, using zirconia (8Zr) and 4 cycles using zirconia precursor plus a last one using aluminosilicate (Al-O-Si) precursor Ref.[11] b) Tensile stress/strain plot of a 3D Skinex® carbon fiber preform-SiC matrix composites prepared by CVI and polyvinylsilane (PVS) infiltration, respectively. Ref.[27]

Tensile measurements show that the mechanical properties achieved through the oxide route are very similar to those the usual SiC CVI process leads to, although the matrix Young's modulus is lower (30 GPa instead of 75 GPa for SiC CVI matrix). A rather pronounced hysteresis in loading-unloading cycles is observed.[11] The same behaviour is observed for composites prepared by combining SiC powder and PVS infiltration.[43] Fig. 6b shows tensile stress/strain plots measured at room-temperature for two materials incorporating the same C-fiber preform (Skinex® from SEP, Le Haillan, France). The loading-unloading hysteresis is related to the mesoporosity of the pyrolysed ceramic. On the contrary, a dense CVI matrix is formed around the fiber and large pores occur between SiC "coated" yarns. In this case, there is no hysteresis but a remanent damage due to the cracking of the dense matrix. We can notice that the composite prepared by the hybrid route keeps a rather constant Young's modulus (35 GPa) whereas those of the CVI processed materials decrease rapidly from 70 to 38GPa with the cracking of the dense CVI deposit.

1.5. Tailoring Simultaneously Different Properties: Functionally Graded Materials (FGM)

By selecting the appropriate sol-gel precursors, the dwell temperature required to achieve maximum densification can be raised or lowered by about 100°C.[6,9] This makes it possible to combine several kinds of impregnated fiber/matrix interphases in the same composite in order to tailor its physical and/or chemical properties for a particular application. As indicated on table I, composites have been fabricated that combine various kinds of woven fibers (SiC Nicalon®, Nextel®, Almax®, Saphikon®) with various kinds of matrices (LAS, mullite, Nasicon, celsian, zirconia)[6-10,12,27] in order to tailor simultaneously thermomechanical and electromagnetic properties.

Mullite is a pure dielectric with a real microwave permittivity close to 5 at 10 GHz but carbon traces originating from the pyrolysis of unhydrolysed organic

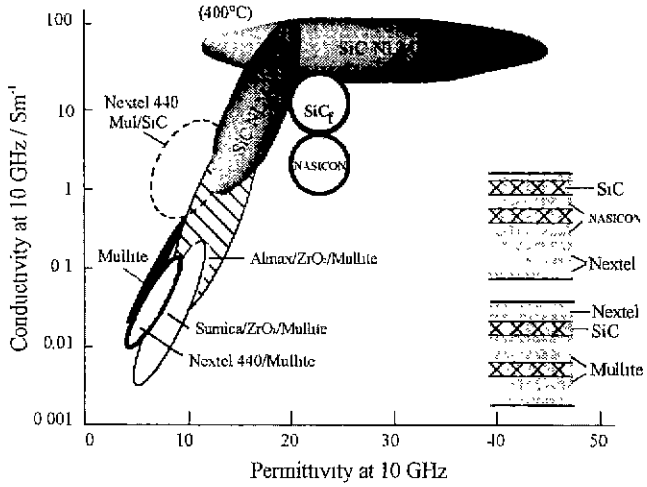

Fig. 7. Conductivity-permittivity at 10 GHz achieved for various composites made by combining or alternating SiC Nicalon®, Al_2O_3 Almax®, Mullite Nextel® or Sumica® fibers with mullite and Nasicon matrices. Data for SiC fiber and sol-gel mullite and Nasicon (x~2) ceramics are given. Ref.[13]

branches of the sol-gel precursors lead to a residual conductivity larger than measured in mullite ceramics synthetized using common sintering routes.[8] The Nasicon solid solution, a solid electrolyte with the structural formula $Na_{1+x}Zr_2Si_xP_{3-x}O_{12}$ ($0 \leq x \leq 3$) offers the advantage of an electrical conductivity varying by four orders of magnitude as a function of x. Furthermore, this material exhibits the rather low thermal expansion required for a composite matrix reinforced with SiC or mullite fibers.

The conductivity of as-received SiC Nicalon NLM fibers is close to 10^{-1}S/m with a real permittivity of ~20 at 10 GHz.[8] Conductivity increases with annealing temperature due to the progressive aromatisation and then the graphitisation of the carbon nanophase dispersed in the SiC matrix.[17] The reaction between SiC Nicalon fibers and an alkali- or earth-alkali containing matrix promotes the formation of a thin carbon-rich interfacial layer (60-100 nm) referred to as the carbon interphase.[3] This interfacial layer contributes significantly to the whole microwave conductivity of the composite.[8] Replacement of the usual glass-matrix by (earth)-alkali free matrices like mullite prevents the formation of such a C film at the interface and helps to control the microwave properties. Thus, microwave permittivity and conductivity of fiber reinforced composites can be decreased by the use of (earth)-alkali free interphase. Additionnally annealing in air at temperatures higher than 700°C for porous matrices and higher than 1200°C for dense oxide matrices makes possible to ajust the conductivity by controlled oxydation of carbon traces.[8,13] Examples of the microwave/conductivity sets achieved by using various fibers, matrices and interphase are given in Fig. 7.

2. Matrix, Fiber and Interphase Characterization

2.1. Depth-Sensing Microindentation

The measurement of local mechanical properties is an important step in the understanding of the macroscopic behaviour of composites. The indentation hardness test is probably the simplest method of measuring the mechanical properties of materials. The use of load-controlled depth-sensing hardness testers which operate in the (sub)micron range enables the study of each component of the composite.

2.1.1 Bulk Properties

Following the work of Loubet et al.,[44] Young's modulus (E) and Vickers microhardness (H_v) can be extracted from the unloading part of load-displacement plots. Typical applied load-penetration depth plots are shown in Fig. 8 for the indentation of a tetragonal-zirconia-reinforced-mullite matrix. E and Hv values are calculated using Loubet's model

$$E = \frac{\partial F}{\partial h}\left(\frac{\pi}{2}\right)^{1/2}\frac{1}{2\sqrt{2h_p}\tan\theta} \quad (1)$$

$$\text{and } H_v = \frac{F\cos^2\theta}{4h_p\sin\theta} \quad (2)$$

2θ being the angle of the Vickers pyramidal indenter and $h_p \simeq h_m$ the plastic depth deduced from the intersection between the extrapolation of the straight line occuring when the load is lowered (unloading cycle) and the abscissa (Fig. 8). At very small penetration depth the measurement error is increased, due to the diamond tip geometrical imperfection and to the difficulty of determining accurately the contact point, (F=0 origin). Furthermore, higher mechanical properties are expected at the nanometric scale, intrinsecly (absence of defects in the analyzed area) or extrinsecly (the densification of ceramics is enhanced at the surface which is a sink for mobile defects). At high penetration depth, cracks may occur, deforming the unloading trace. Thus the observation of a plateau on E(Hv) plot vs hm is mandatory for the determination of the true E and Hv values (Fig. 8). This method is well-suited to analyze the various phases constituting a composite providing that the area of constituting phases reaches at least 2-4 μm^2. For instance, the Young's modulus of the silica-rich mullite glass surrounding the fibers, arising from of the thermal treatment of the alumino(boro)silicate interface precursor is ~90 GPa (H_v ~8GPa).[10] This low value corresponds to that usually measured for glass-ceramics.[45] Larger E and Hv values are observed for zirconia containing mullite matrix.

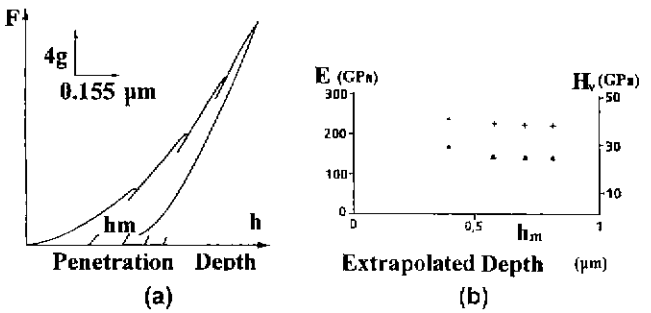

Fig. 8. Representative indentation plot of applied load (F) as a function of diamond tip penetration depth (h) in the matrix (mean composition $6Al_2O_3 4SiO_2 ZrO_2$) for a composite hot-pressed at 1350°C (a). Partial unloadings are made in order to determine the Vickers microhardness Hv and the Young's modulus E as described in Ref. 17; the H_v (triangle) and E (cross) values are deduced from the plateau observed in the plots given on the right (b).

Indentation of a fiber allows one to observe the degradation of the fiber properties as a function of processing and thermal ageing. For instance, no degradation is evident in mullite matrix composites prepared below 1300°C: E and Hv values remain unchanged (E~220 GPa; H_v~25 GPa). On the other hand, the indentation of fibers in composites sintered above 1300°C shows a lowering of both Young's modulus and micro-hardness.[10]

2.1.2. Fiber/matrix Interface Properties

The high strength and toughness of (glass)-ceramic matrix composites result directly from the low fiber-matrix bonding originating in the processing. Usually, a reaction between SiC Nicalon fibers and an alkali- or earth-alkali-containing matrix leads to the formation of a thin carbon-rich interfacial layer (~100 nm) referred to as the carbon interphase.[1,3,46] This interphase acts as a "fuse", deflecting the matrix microcracks parallel to the fiber axis and thus avoiding the early failure of the fibers.[1] This interphase is formed in situ during the hot-pressing as a result of the fiber-matrix chemical reaction[3,27] or results from the deposit of a thin coating of C, BN, SiC, ZrO_2, etc.,[7,47,48] when non-reactive matrices are used. These interfaces/interphases have been extensively studied by electron microscopy.[3,48-50]

Another important parameter controlling the fibermatrix bonding is the sign and the level of the residual mechanical stresses in the composite arising after processing from the mismatch of fiber and matrix coefficients thermal expansion. If it is too high, a radial compressive residual stress increases the fiber-matrix bonding and is usually detrimental. A significant stress is however required to promote the load transfer around broken fibers and to ensure a protection of the fibers against atmosphere corrosion. The sliding strength is usually measured on 1D composites using instrumented or non-instrumented micro-hardness testers following the Marshall's method.[51-54] If the applied load exceeds the threshold load (Fs) (Fig. 9), the fiber slides within the matrix and a step becomes visible at the fiber periphery: after indentation, part of the fiber push-down is permanent. This makes it possible to study the fiber/matrix mechanics. The fiber to be tested must be in axial position (circular section on the polished section of the composite) and have a uniform arrangement of distances from neighbouring fibers. Its diameter is measured. If the indent is not centered or if there is the least sign of fiber splitting, the measurement is discarded. Example of applied load indentor/tip displacement is given in Fig. 9. Three regions can be clearly dis-

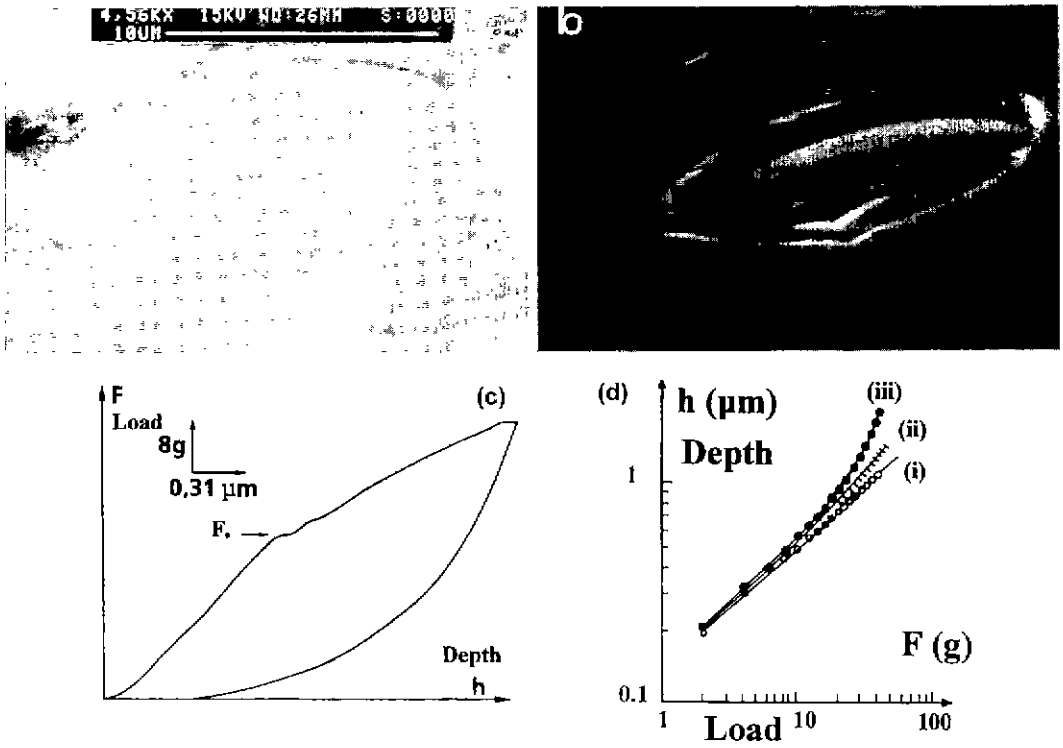

Fig. 9. SEM photomicrographs showing a SiC Nicalon indented fiber in Nasicon (a) and LAS, a β spodumene rich glass ceramic (b) matrix composites: see the circonference step due to the fiber debonding and sliding; Typical indentation plot of applied load (F) against penetration depth (h) for representative SiC fiber embedded in a Nasicon ceramic matrix (c). The arrow corresponds to the debonding threshold and the onset of the sliding regime. Log/log plot highlighting the fiber sliding experimental data from the indentation plots (d) for three different SiC NLM202 fibers in Nasicon matrix with (ii, iii) or without (i) sliding.

tinghished on the load (F)-depth (h) plots:

i) the first polynomial regime, following the so-called Meyer law

$$h = \alpha F^{\beta} \tag{3}$$

giving a straightline on log-log plots related to the fiber indentation and showing elastoplastic deformation under the sharp indenter,

ii) a region characterized by a lower rate of load increase, a few steps being often observed at the limit between the elastoplastic response of the fiber and the debonding-plus-sliding regime (F_s is called the sliding force),

iii) a third region can be observed when the pyramidal diamond tip comes into contact with the matrix ($F>>F_s$). Conispherical or cylindrical diamond can be used to avoid this drawback in the case of small diameter fibers. In some cases, e.g. when big fibers are used, the sample can be made thin enough to measure the fiber push-out length.[54,55]

The interfacial frictional stress (τ) related to sliding may also be measured in 2D materials, if the fiber curvature is larger than the debonding length induced by fiber sliding.[8,10] For instance, the very large yarn curvature in 4-direction woven fabrics (curvature radius > a few tens of centimeters whereas debonding length ranges between 50 and 500 µm, typically e.g.) makes experiments and calculations possible.[10] First calculations of the interfacial stress (or sliding strength) τ have been made using Marshall's uniaxial model.[52] The elastoplastic contribution of the fiber before the sliding threshold (Fo sliding: threshold load) is assumed to follow a Meyer law[18]:

In the sliding regime $F > F_s$, h: penetration depth, F: applied load

$$h = \alpha F^{\beta} + \frac{(F - F_s)^2}{4\pi^2 r^3 E\tau} \tag{4}$$

E: Young's modulus, r: radius of the fiber, respectively.

Numerous models have been proposed.[51-61] In fact, it is very difficult to determine the true interfacial frictional stress and to compare the τ values calculated by different authors. Only comparative studies using the same model -and the same apparatus- are reliable. A criterion for choosing among different models is the height of the residual step after indentation.[18] However, the measurement is difficult and the thermally induced stress should also be taken into consideration.[56]

Comparative analysis (using same model and instrument) made on SiC/LAS, MLAS (L for lithium oxide, A for aluminum oxide, S for silicon oxide, M for magnesium oxide) and mullite matrix composites shows that τ and F_s values measured on composites without carbon fiber-matrix interphase remain larger (τ~20-30 MPa, F_s~10-25 g) than those measured on composites with a well-formed carbon film (τ~3-8 MPa, $F_s \leq 2$ g). For the latter, a large

increase in the τ value is observed after annealing in air, due to the burning of the carbon interphase and the formation of a rigid silica interphase.[2,3,60]

2.2. Micro-Raman Spectrometry

Like other vibrational spectroscopies, Raman scattering can be used to study the short-range structure of any solid, either amorphous or crystalline. Indeed, the wavenumber and bandwidth of Raman spectra depend on the atomic range order in a material. The plot of the Raman intensity can be used to follow the evolution of the scatterers content, as a function of thermal treatments,[16] for instance. Once the Raman spectra of bare fibers subjected to given thermal treatments are known, comparison can be made with the spectra of fibers embedded in the composite matrix, for which reactions can occur at the interface.[16,17] Examples discussed hereafter have been chosen among composites made of Graphil LXA® carbon fibers and of NLM202 Nicalon® and Hi-Nicalon® fibers embedded in various oxide matrices (mullite, NASICON).

During the last years, micro-Raman spectroscopy has been used increasingly as a powerful technique to measure local residual stress in submicronic electronic devices.[57-59] Such localized stresses can induce various types of structural defects modifying the electronic properties. As pointed out in § 2.1, knowledge of the stress concentrations in fiber reinforced composites is of major importance. Since such stress concentrations cannot be measured easily, many analytical theories have been proposed to understand the micromechanics of composites at the light of the microindentation push-in and push-out tests. First, Galiotis *et al.* and Young *et al.* demonstrated that Raman spectroscopy is an excellent method to follow the deformation of aramid fibers.[60-62] This is a result of the variation of the (stretching) vibrational wavenumber, as a consequence of the anharmonicity of the interatomic bonds.[63,64] The relationship linking Raman wavenumber shifts (Δν) to the tensile strain (Δε) is linear.[60]

$$\Delta\nu = J \times \Delta\varepsilon \qquad (5)$$

Knowledge of Young's modulus (E), found in the literature or obtained from local microindentation measurements (see above § 2.1) allows calculation of the corresponding stress distribution. A shift towards higher energies indicates a compressive strain, whereas a tensile strain corresponds to a decrease in energy. Kevlar fibers display an exceptional strength/stiffness in tension and modulus softening followed by abrupt "yielding" in compression. On the contrary, in tightly bonded inorganic materials e.g. SiC, the $|\Delta\nu| = J \times |\Delta\varepsilon|$ relationship is symetrical: Fig. 10 shows the correlation of J values (based on first order Raman spectra) with Young's modulus for different kinds of carbon containing fibers.[63] Absolute J values decrease with increasing Young's modulus. This can be related to the decrease of the bond

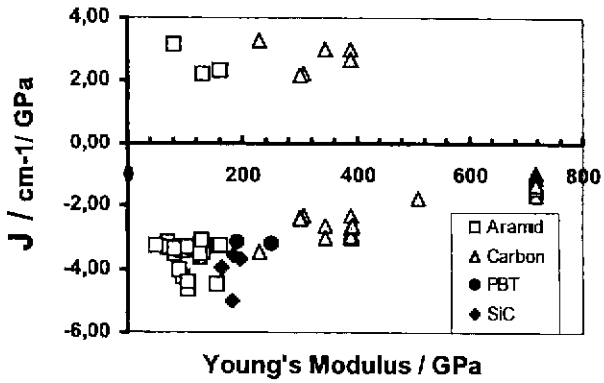

Fig. 10. Correlation between the tensile Raman shift slope (J) and the Young's modulus (E) for different kinds of carbon containing fibers. Ref.[63]

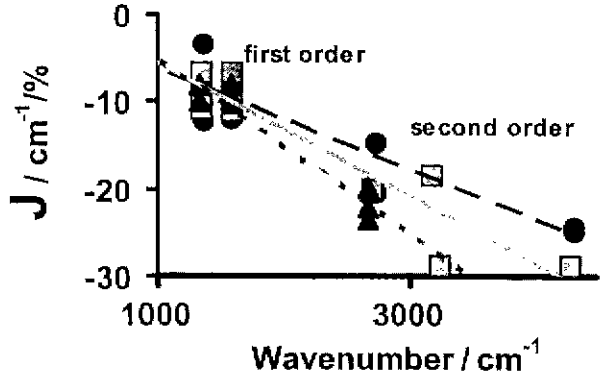

Fig. 11. Plot of the tensile Raman shift slope (J) measured for FT700 carbon fibers as a function of the Raman (first order, second order or combination) bands for various exciting lines (triangle: 632 8 nm, square: 514.5 nm; circle: 457.9 nm). Ref.[63]

anharmonicity. In the case of an anharmonic potential, the wavenumber shift increases when high order transitions are studied. Consequently, high-order Raman bands may be prefered for the measurement of stress-induced shifts. Fortunately, carbon bonds are present in many fibers and their absorption in the UV-visible range gives rise to a (pre)resonance Raman phenomenon, enhancing the second-order or even the third-order spectra. Fig. 11 compares the J values determined for different carbon fibers using first order, second order and combination peaks. The interest in using high order spectra, whatever the required increase of recording time, is obvious.

2.2.1. Evolution of Fiber Nanostructure with Temperature and Fiber-Matrix Reaction

It is well documented that crystalline graphite has a strong peak at about 1580 cm^{-1} resulting from the in-plane stretching of the sp^2 bonded carbon (C=C double bond). On the other hand, the diamond spectrum consists of a peak at 1331 cm^{-1} characteristic of sp^3-bonded carbon, the lower wavenumber arising from a longer C-C single bond.[15,65-68] The study of disordered "diamond/gra-

phite' by many techniques has demonstrated that disordered carbons are made of different C-C bondings,[65-68] which explains the broad C-C fingerprint of carbon containing materials. A spectral line shape analysis and decomposition is needed to determine the wavenumber and width and to check the wavenumber shift under tensile (compressive) stress. Fig. 12 shows typical (first order) Raman spectra of Hi and Hi-S SiC Nicalon® fibers supplied by Nippon Carbon. The spectra of "SiC" fibers mainly consist of two broad peaks at about 1350 and 1600 cm^{-1}, assigned to the sp^3 and sp^2 bonded carbon of the carbon nanoprecipitates and to the sp^3 bonded carbons of the (oxy)carbide second phase, binding SiC and C moieties.[15,17,69-74] A broad band around 1530 cm^{-1} has been assigned to sp^2 bonded atoms, disordered by neighbouring heteroatoms or nanoporosity,[15] a 1630 cm^{-1} band appears to be characteristic of graphitic precipitates.[15,17,70] An additional broad band around 1140 cm^{-1} might be due to disordered and hydrogenated sp^3 bonded carbons. The proper fingerprint of SiC, the major consituent of the SiC fiber, is neither visible on the spectrum of as-received NLM and Hi Nicalon® SiC fibers, nor on that of fibers heated below 1300°C[15-17]; it consists of two main bands at 796 and 973 cm^{-1} [71] as seen on the core spectrum of the Hi-S Nicalon fiber (Fig. 12), a quasi stoichiometric SiC fiber. However, owing to their optical absorption in the visible range, the Raman scattering efficiency of carbon species is at least ten time that of SiC. Consequently, SiC crystallites may be present well before their fingerprint is observed on the Raman spectra. The penetration depth of the laser beam in SiC fibers can be assumed to be about 0.1 μm or less.[17] Structural differences between NLM, Hi and Hi-S Nicalon grades are straightforward. For instance, the bandwidth of the sp^3 bonded C-C stretching mode measured on the above fiber surface is 180, 70 and 65 cm^{-1}, respectively.[17] The values measured on the fiber core, on a fracture (or on a polished section), are slightly larger, which confirms the difference previously pointed out by other methods between fiber core and surface: SiC bands are observed only for the core spectrum of a HiS Nicalon® fiber (Fig. 12). This indicates that the content of C-C bond in this fiber is lower than for the other grades but the high intensity of the sp^3/sp^2 doublet indicates that the fiber remains non-stoichiometric (Si/C<1), the excess of carbon being larger at the fiber surface. The very low intensity of the 1530 cm^{-1} band on the core spectrum is consistent with a very low oxygen content in the Hi-S Nicalon® fiber. Fig. 13 shows the wavenumber shifts as a function of the annealing temperature. The spectra have been recorded with the same laser beam power and recording time.[17] The monotonous wavenumber increase of the sp^3 C-C mode of NLM Nicalon® fibers above 1000°C indicates that the aromaticity of the carbon bond increases. This is confirmed by an increase of the conductivity.[17] The frequency decrease of the sp^2 C = C mode above 1600°C is consistent with the evolution of carbon moieties

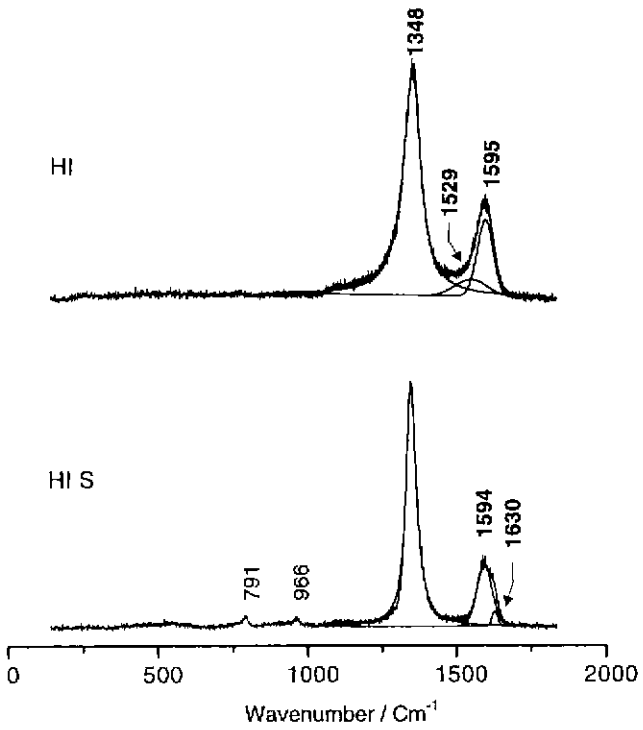

Fig. 12. (First order) Raman spectra of the core of desized Hi and Hi-S Nicalon® SiC fibers recorded under 2 mW laser beam for 90s (514.5 nm exciting line).

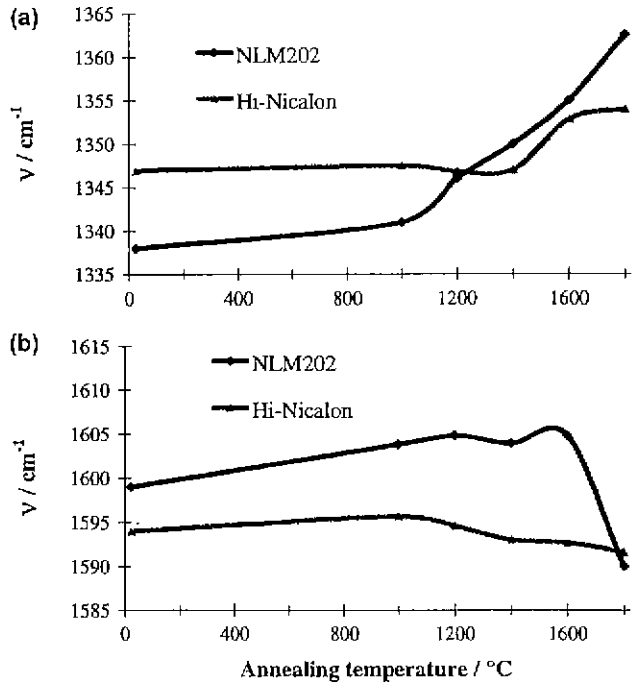

Fig. 13. Wavenumber plots of the sp^3- (ca. 1350 cm^{-1}) (a) and sp^2-bonded (ca. 1600 cm^{-1}) (b) carbon bands of (desized) NLM202 and Hi-Nicalon® SiC fibers (core) measured at room temperature as a function of annealing temperature (dwell 30min). Spectra were recorded under 2 mW laser beam power (90s recording time). Ref.[17]

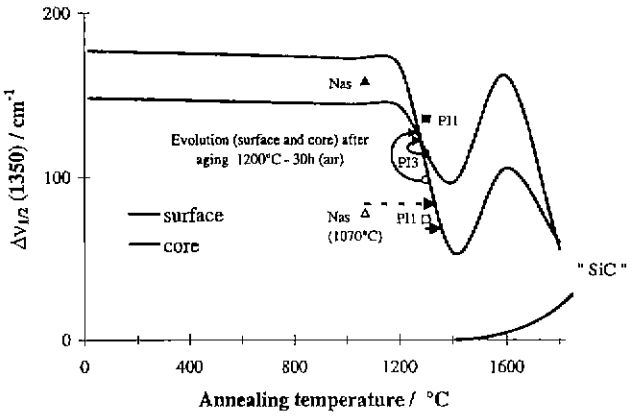

Fig. 14. Bandwidth evolution versus thermal treatment in reducing atmosphere of a desized NLM202 SiC Nicalon fiber (spectra are recorded at R.T.). Differences between the surface (S T<1100°C) and the core (C) of the fiber are given. The curve called "SiC" illustrates the intensity evolution of the SiC Raman fingerprint. Data recorded on the surface of fibers embedded in a Nasicon matrix interphase (triangle, sintering temperature 1070°C) and in a mullite interphase (square, circle using various interface precursors, sintering temperature 1300°C) are given. Evolution after ageing at 1200°C, 30 h, in air, is shown.

toward true graphitic particles, as deduced from the band shape and intensity analysis. The thermal evolution of the Hi-Nicalon® fiber is different from that of the NLM. In the Hi-Nicalon® there is no change in wavenumber before 1300°C. Its better thermal stability has been explained by the absence of the internal oxydation of carbon moieties observed, for the NLM Nicalon® fiber, between 1000 and 1600°C.[15,73,74]

Fig. 14 compares the plot of the bandwidth of NLM 202 Nicalon® fibers as a function of annealing temperature, in reducing and oxydizing environments. The first environment simulates the effect of processing and the second the ageing in operating atmosphere. The bandwidth remains constant up to about 1200 and 1600°C for NLM and Hi Nicalon® fibers, respectively.[15,17] Above, bandwidth narrowing arises from the onset of the crystallization of the NLM Nicalon® fiber (which leads to a deterioration in the mechanical strength) and the carbon precipitation resulting from the decomposition of the oxycarbide second phase that embeds the SiC and C crystallites in the Nicalon fiber.[73,74] In air, this latter reaction starts at lower temperature. The extent of variations is strongly reduced for the Hi-Nicalon® grade.

2.2.2. Fiber Degradation Control in Ceramic Matrix Composite

Fig. 15 shows typical spectra recorded on the core and at the periphery of polished sections of fibers embedded in various oxide matrices. The bandwidth narrowing observed for the fiber region near the fiber/matrix interface is obvious. On the other hand, the bandwidth measured on the fiber core corresponds well to the value expected from the thermal evolution given on Fig. 14 for bare fibers.

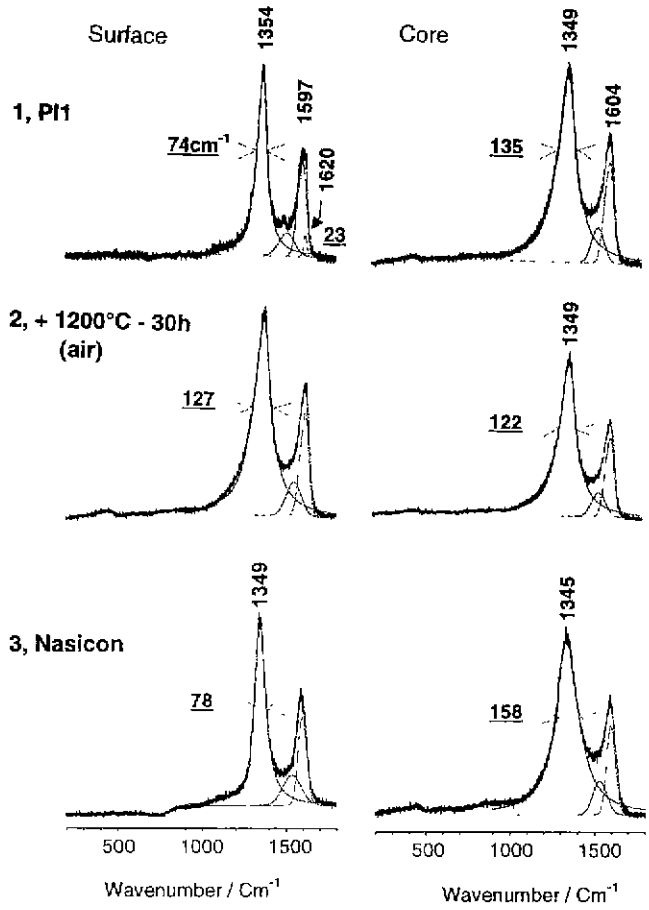

Fig. 15. Raman spectra of polished sections of NLM202 SiC Nicalon fibers in various matrices in the carbon bond stretching region. Ref.[17]: 1, mullite matrix associated to an aluminoborosilicate interphase precursor (PI1, hot-pressing temperature 1300°C, reducing atmosphere); 2, mullite matrix and an optimized aluminoborosilicate+zirconogermanate interphase. The composite has been hot-pressed at 1300°C in reducing atmosphere and post-annealed at 1200°C in air, 30 h,[10] Nasicon matrix and zirconophosphosilicate interphase, sintering temperature 1070°C.[8]

A wavenumber shift is often observed. This wavenumber shift could be due to i) chemical or structural evolution of the materials or ii) stress/strain induced by the presence of various phases in the same material (see § 3.4).

The wavenumber shift induced by local heating should be constant for a given power of illumination. Consequently, comparison can be made for data obtained using a common procedure. The distinction between the wavenumber shift caused by chemical and structural modifications and the one that is due to compression or tensile load is not obvious. For these reasons, the information deduced from bandwidth evolution must be taken into account and comparisons should not rely on the wavenumber shifts only. Additional information can be extracted from the band intensity. Furthermore, comparison between wavenumber measured on the fiber core and at the fiber surface can help the understanding of the fiber state.

Raman analysis capabilities can be illustrated by comparing three different woven fiber reinforced-ceramic matrix composites (Fig. 15):

• Composite #1 consists of NLM 202 SiC woven fibers embedded in a mullite ($3Al_2O_3 \cdot 2SiO_2$) matrix hot-pressed at 1300°C for 45 min. An aluminoborosilicate gel interface precursor (interface precursor n°1) has been used to tailor the densification.[6,17]

• Composite #2 has been prepared in the same way but using a more complex gel interface precursor. Ageing has been simulated by 30h annealing in air at 1200°C.[10]

• Composite #3 consists of NLM 202 SiC woven fibers embedded in a NASICON matrix ($Na_{2.9}Zr_2Si_{1.9}P_{1.1}O_{12}$, a superionic conductor chosen for its microwave properties) and hot-pressed at 1070°C for 45 min.[8] A gel precursor leading to a thick glassy zirconophosphosilicate interphase is used to limit the SiC fiber attack by sodium ions of the NASICON matrix.

For instance, comparison of the sp3 bonded carbon wavenumbers measured at core for fibres of composite 1 and 2 shows a rather constant value (ca. 1349 cm^{-1}) equal to that given by the plot of Fig. 13 for a fibre thermally treated at 1300°C. This indicates that the fibre core evolution only depends on the thermal treatment temperature. The small variation of the bandwidth is normal considering the dispersion in fibre diameter and fibre location in the composite. On the contrary, the 74 cm^{-1} bandwidth measured on composite 1 at the fibre periphery corresponds to the smallest values we measured on bare NLM fibres, when these fibers had been heated in reducing atmosphere. The absence of SiC bands on the spectrum indicates that the fibre is in a state rather similar to that obtained by heating at 1400°C. The interface precursor #1 enhances the degradation of the fibre. The observation of the 1620 cm^{-1} band, characteristic of graphite phase, shows that "large" (i.e. $\geq$10 nm) and "well crystallized" graphitic particles are formed at the fibre surface. The bandwidth measured near the fiber on the composite #2 prepared with an optimized interface surface is equal to that of the core, which indicates that the surface degradation of the fiber is limited. On the contrary, analysis of a fiber embedded in a NASICON matrix points out large differences between core and periphery spectra. The bandwidth of the sp^3 bonded carbon band is only 78 cm^{-1} in fibre periphery. This corresponds to the lowest value measured on reference plot of Fig. 13, although the sintering temperature is only 1070°C. On the other hand, the bandwidth measured on the fibre core is about 160 cm^{-1}, which is consistent with a thermal treatment at 1070°C. Accordingly, microhardness analysis shows that SiC fibre core retains initial mechanical properties.[8]

2.2.3 Fiber Degradation in Metal Matrix Composites (MMC's)

Continuous fiber reinforcement of a metal matrix composite is made using large-diameter "SiC" fibers produced by chemical vapor deposition. Among this kind of fibers, the SCS-6, Textron® fiber has received considerable attention. It consists of a monofilament carbon core, nominally 33 μm in diameter with a β-SiC sheath radially grown by a CVD process. In this sheath, an inner SiC zone approximately 16 to 38 μm from the fiber center and differentiated from the outer SiC zone by an optically visible mid-radial boundary showed excess carbon.[75,76] In order to control chemical reaction between SiC and the metal matrix (titanium alloy) during processing of the composite, the fiber is coated with carbon layers.

Fig. 16 shows a representative Raman spectral line scan (2 μm step) recorded from the fiber/matrix interface to the fiber center.[77] The matrix is a Ti6242 alloy prepared by foil-fiber-foil hot-pressing at 960°C.[78] Four zones are straightforward: i) the pure carbon outer coating (scan 1-3). The high fluorescence background (scan 3) can be attributed to a highly porous region or a crack between the fiber and the matrix capturing polishing aid residues, ii) the pure SiC outer zone (scan 4-16, see the broad SiC fingerprint between ca. 750 and 970 cm^{-1}, characteristic of heavy faulted SiC),[15] iii) the zone made of highly disordered carbon and SiC (broad component at ca. 1350 and 1600 cm^{-1} with increasing intensity) and iv) the pure carbon core with a narrower doublet. All these

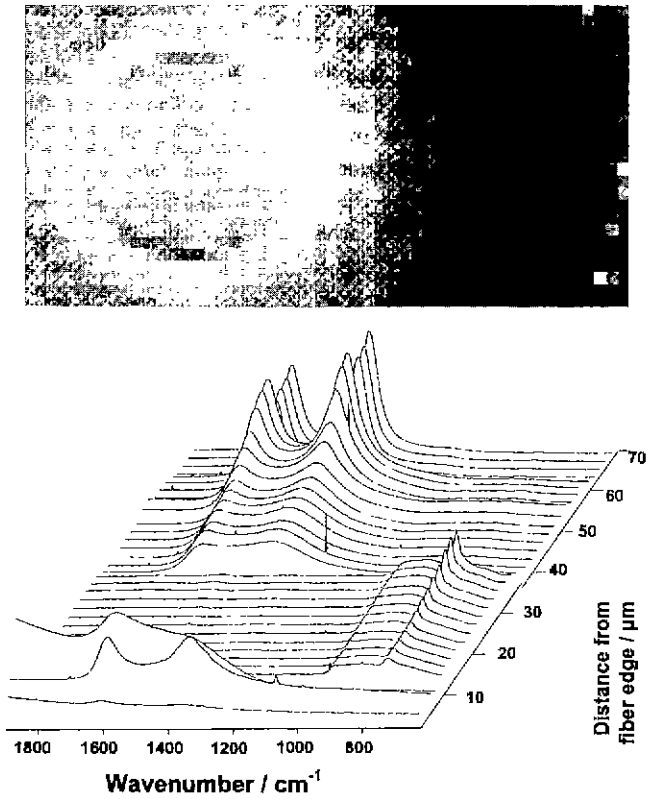

Fig. 16. SCS-6 fiber (140 μm diameter) in a Ti 6242 composite: top, Imaging of the $\nu_{C\,C_{sp^2}}$ Raman peak area: 25 lines, 50 spectra each (2×2 μm step); bottom, Spectral line scan from the fiber/matrix interface to the fiber core (2 μm step). Ref.[63]

different zones can be observed on the image calculated using the peak area of the 1600 cm^{-1} component (sp^2 hybridized C-C bond). We also note that the carbon bands appear suddenly, which is surprising from a chemical point of view. This can be attributed to the limit of the carbon dissolution in disordered $Si_{1-x}C_{1+x}$ phase.

Comparison with the spectra of a pristine SC-6 fibers makes it possible to evidence the physical-chemical changes induced by the processing. The plot of the fullwidth at half height for the carbon sp^3 stretching is shown on Fig. 17. The shift induced by diffusion of carbon from the core to the SiC CVD coating during the hot-pressing step is straightforward. Plot of the wavenumber of the SiC TO mode shows a significant decrease, indicating that SiC outer coating is under tensile stress in the composite.

2.2.4 Visualisation of the Compressive (Tensile) Strain of the Fiber in Ceramic Matrix

Fiber stress determination is of major importance for the modelisation of composites and it is now well established that Raman microspectroscopy, whose main advantage is to be non-destructive, is most helpful to visualize the deformation of polymeric and carbon fibers embedded in epoxy matrices.[60-62,79-81] It makes it possible to characterize C/C composites[52] and has been recently applied to study the strain distribution to which fibers are subjected in ceramic fiber-reinforced glass[83] or ceramic matrix composites.[84] The only requirement for such studies is to use matrix sufficiently translucent to allow recording of the signals from these fibers through the matrix (a few micron to a few tens of micron inside) and whose spectrum does not overlap that of the fibers. The quantitative information on the fiber strain distribution ensues from a calibration of the "wavenumber shift" of the peak against strain.[16,83] Typically, the first order J Raman wavenumber shift slope is ~10 cm^{-1}/% for high modulus carbon fibers, ~7 cm^{-1}/% for high strength carbon fibers, ~4 cm^{-1}/% for the NLM202 Nicalon® fiber and ~3 cm^{-1}/% for the Hi-Nicalon fiber. It is of prime importance to carry out wavenumber-strain calibrations on fibers that are heat treated to simulate the composites' elaboration process, since it has been pointed out that the significant surface (and even core) evolution SiC fibers undergo during this elaboration induces wavenumber and band-width shifts of the Raman peaks.

Fig. 18 shows the Raman wavenumber shift as a function of the position for a Graphil LXA fiber embedded in a pseudo-mullite matrix (a mixture of α-alumina and silica) hot pressed at 1550°C.[84] A distance of 1.25 μm between the measuring points was respected. Given that the aluminosilicate matrix has a very weak Raman effect and that the matrix layer above the fiber surface was rather thin, the Raman signal came only from the fiber surface. The compressive effect is obvious.

2.2.5 Determination of the true Thermal Residual Stress (Strain)

The thermal residual strain (Δε) induced by the matrix on the fibers can be calculated using the thermal expansion coefficients (α) assuming a blocking temperature (T_b) close to the elaboration temperature

$$\Delta\varepsilon = (\alpha_{matrix} - \alpha_{fiber})(T_b - T_{RT}) \quad (8)$$

This model supposes that the coefficients of thermal expansion (CTE) of the fiber/matrix in the composite are equal to those of the pristine fiber and of pure ceramics having the composition of the matrix. Such a calculation does not take into account the likely radial compression (the measurement of the radial CTE of fibers is not obvious) and shrinkage of the fiber, nor any possible

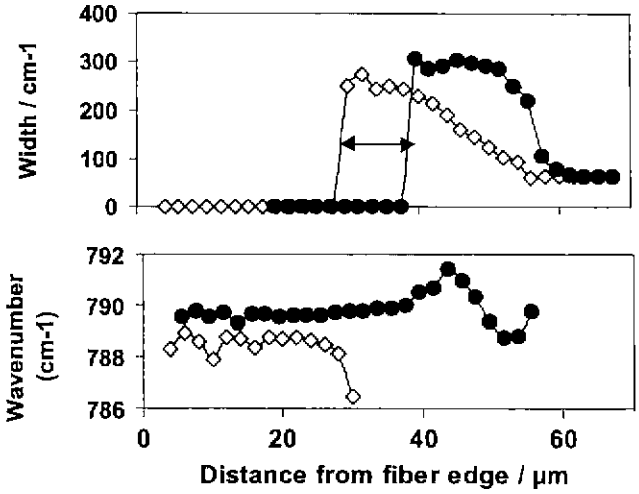

Fig. 17. Typical spectral informations recorded for a SCS-6 fiber, according to the distance to its interface with a Ti6242 alloy matrix (lozenges) and for a pristine fiber (black circles) : on top, full width at half height for the carbon "sp^3" band; on the bottom, SiC TO mode wavenumber. Ref.[63]

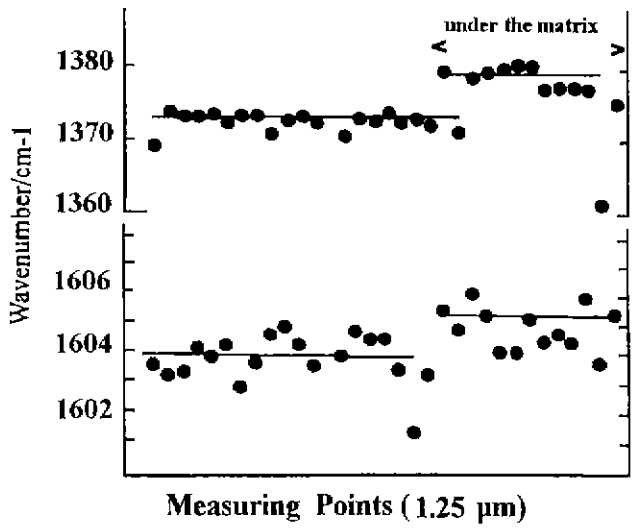

Fig. 18. Wavenumber jump of the sp^3 (top) and sp^2 (bottom) C-C bonds recorded on a Graphil LXA carbon fiber gradually embedded in a pseudo mullite matrix. Ref.[84]

Table 2. Comparison between Δε Calculated from Raman Measurements of from the Thermal Expansion Coefficients (α); (negative sign for a compression of the fibers) (after[63])

Fibre	T_F (°C)	$\Delta\varepsilon_{Raman}$ (%)	α_F (10^{-6}/K)	α_M (10^{-6}/K)	$\Delta\varepsilon_\alpha$ (%)	Remarks
Graphil*	1300	-0.26/-1.33	≃0	4.1	-0.53	Matrix microcracks
NLM207**	1550	0.75/2.5	3.1	4.8	-0.27	Crack-free matrix
Hi***	1250	-0.47/-1	3.5	4	-0.06	Isolated fiber

*LXA® carbon fiber (Courtauld, UK), pseudo mullite matrix[40,81], **Nicalon© SiC fiber (Nippon Carbon, Japan), mullite matrix[84]
***Nicalon© SiC fiber (Nippon Carbon, Japan), mullite matrix[16]

CTE anisotropy.

Table II gives a comparison between Δε calculated from Raman measurements and from thermal expansion coefficients. A negative sign corresponds to a compression of the fibers. Values given for the Raman shift have been calculated taking into account the possible deviation arising from the J slope uncertainty as function of the Raman peak used for the measurement.[16,84] A rather good agreement is found for the Graphil LXA carbon fiber/mullite composite, where for both methods the fiber are under compression. On the contrary, Raman analysis indicates a tension of the NLM207 fibers embedded in a mullite matrix, although thermal expansion modeling indicates a compression. The lack of microcracks in the matrix is more consistent with the Raman measurements.

IV. Summary

The examples reported in this paper show that the new processing routes using liquid organometallic ceramic precursors allow the tailoring of multiphase and composite materials at the micro- and nanoscale and hence the development of functionally graded materials. The stringent advantages are a better control of the matrix shrinkage during the densification, the flexibility of the matrix composition from some mixtures of precursors, a reduction of the cost and of the processing time in comparison with the CVI technology.

Depth-sensing microindentation allows the reliable determination of Young's modulus, Vickers microhardness and fiber sliding threshold force and produces comparative data of the interfacial shear stress.

Variations in chemical bonding and short-range order can be extracted from the Raman peaks intensity, wavenumber and bandwidth, in order to gain a better understanding of the fiber evolution during the composite preparation and its ageing in operating atmospheres. The wavenumber shifts can be used to map the strain (and calculate the stress). Analysis of the bandwidth offers a tool to ascertain whether the wavenumber shift is strain induced or related to structural evolution of the Raman probe.

Acknowledgment

The author wishes to thank Dr. M. Parlier for helpful discussions, Doctors E. Mouchon, E. Bruneton, S. Karlin, V. Vendange, M. Wey and MM. J.L. Lagrange, C. Courtemanche and G. Gouadec for their contribution.

References

1. K. K. Chawla, "Ceramic Matrix Composites," Chapman and Hall, London, 1993.
2. N. J. Jacobson, E. J. Opila, D. S. Fox and J. L. Smialek, "Oxidation and Corrosion of Silicon-based Ceramics and Composites," *Mater. Sci. Forum*, **251-254**, 817-832 (1997).
3. Ph. Colomban, "The Corrosion of Ceramic-Matrix Composites," *Mater. Sci. Forum* **251-254**, 833-844 (1997).
4. R. Naslain and F. Langlais, "CVD Processing of Ceramic-Ceramic Composite Materials." *Mater. Sci. Res.*, vol. 20, Plenum Press, New York 145-164 (1985).
5. T. M. Besman, R. A. Lowden and D. P. Stinton, "Overview of Chemical Vapor Infiltration"; pp. 215-229, in *High Temperature Ceramic Matrix Composites*, Proc. HT-CMC1-6thEACM. R. Naslain, J. Lamon, D. Doumeingts, Woodheat Pub. ENired by, Abington Cambridge (UK), 1993.
6. Ph. Colomban, M. Menet, E. Mouchon, C. Courtemanche, M. Parlier, "Composites Céramique-Céramique Multicouches Elaborés en Utilisant un Précurseur d'Interface et un Précurseur de Matrice," French Patent ONERA FR 2672283 (7/4/92), European Patent EP92400235-5 (18/12/96), US Patent 7930804.
7. E. Mouchon and Ph. Colomban, "Oxide Ceramic Matrix-Oxide Fibers Woven Fabric Composites Exhibiting Dissipative Fracture Behavior," *Composites* **26**, 175-182 (1995).
8. E. Mouchon and Ph. Colomban, "Microwave Absorbent: Preparation, Mechanical Properties and RF/Microwave Conductivity of SiC (and/or mullite) Fibers Reinforced NASICON Matrix Composites," *J. Mater. Sci.* **31**, 323-334 (1996).
9. Ph. Colomban, "Process for Fabricating a Ceramic Matrix Composite Incorporating Woven Fibers and Materials with Different Compositions and Properties in the Same Composite," *Mater. Tech.* **10**, 89-103 (1995).
10. Ph. Colomban, E. Bruneton, J. L. Lagrange and E. Mouchon, "Sol-Gel Mullite Matrix-SiC and -Mullite Woven Fabric Composites with or without Zirconia-containing Interphase: Elaboration and Properties," *J. Eur. Ceram. Soc.* **16**, 301-314 (1996).
11. Ph. Colomban and M. Wey, "Sol-Gel Control of Matrix Net-shape Sintering in 3D Fiber Reinforced Ceramic Matrix Composites," *J. Eur. Ceram. Soc.* **17**(12), 1475-1483, 1997.

12. J. L. Lagrange and Ph. Colomban, "Double Particle Reinforcement of Ceramic-Matrix Composites Prepared by a Sol-Gel Route," *Composites Sci. & Techn.* **58**(5), 653-658 (1998).
13 Ph. Colomban, "Sol-Gel Control of the Micro/Nanostructure of Functional Ceramic-Ceramic and Metal-Ceramic Composites," *J. Mater. Res.* **13**(4), 803-811 (1998).
14 Ph. Colomban and V. Vendange, "Sol-Gel Routes Towards magnetic Nanocomposites with Tailored Microwave Absorption," Proc. MRS Fall Meeting, 1-6 dec. 1996. *Nanophase and Nanocomposite Materials* II, S. Komarneni, J. C. Parker and H. J. Wollenberger eds, vol **457**, 451-462 (1997).
15. S. Karlin and Ph. Colomban, "Raman Study of the Chemical and Thermal Degradation of As-received and Sol-Gel Embedded Nicalon and Hi-Nicalon SiC Fibers used in CMC's," *J. Raman Spectrosc* **28**, 219-228 (1992).
16. G. Gouadec, S. Karlin and Ph Colomban, "Raman Extensometry Study of NLM202® and Hi-Nicalon© SiC Fibers," *Composites Part B* **29B**, 251-261 (1998).
17. S. Karlin and Ph. Colomban, "Micro-Raman Study of SiC Fiber-Oxide Matrix Reaction," *Composites Part B* **29B**, 41-50 (1998).
18. J. L. Lagrange, B. Passilly, M. Parlier and Ph. Colomban, "The Determination of local Mechanical Properties in CMC's"; pp. 241-252, Proc. JNC-8, *Comptes Rendus des 8emes Journées Nationales sur les Composites*, 16-18 Nov. 1992, Palaiseau (France), Edited by O. Allix, J. P. Favre and P. Ladeveze, AMAC, Paris, 1992.
19. Ph. Colomban, "Gel Technology in Ceramics, Glass-Ceramics and Ceramic-Ceramic Composites," *Ceramics Int.* **15**, 23-50 (1989).
20. L. C. Klein (ed.), "Sol-Gel Technology," Noyes Publication, Park-Ridge NJ, 1988.
21. V. Vendange and Ph. Colomban, "Determination of the Hydroxyl Content in Gels and porous "Glasses" from Alkoxide Hydrolysis by combined TGA and BET Analysis," *J. Porous Mat.* **3**, 193-200 (1996).
22. V. Vendange and Ph. Colomban, "How to tailor the porous Structure of Alumina and Aluminosilicate Gels and Glasses," *J. Mater. Res.* **11**(2), 518-528 (1996).
23. V. Vendange and Ph. Colomban, "Densification Mechanisms of Alumina, Aluminosilicates and Aluminoborosilicates Gels, Glasses and Ceramics," *J. Sol-Gel Sci. Technol.* **2**, 407-411 (1994).
24. Ph. Colomban and V. Vendange, "Sintering of Alumina and Mullite Prepared by Slow Hydrolysis of Alkoxides: the Role of Protonic Species and of Pore Topology," *J. Non-Cryst. Solids* **147/148**, 245-250 (1992).
25. S. Yajima, K. Okamura, J. Hayashi and M. Omori "Synthesis of Continuous SiC Fibre with a High Tensile Strength," *J. Am. Ceram. Soc.* **59**(7-8), 324-327 (1976).
26. P. Noireaux, J. Jamet, M. Parlier and M. P. Bacos, "Polysilanes et leur Procede de Preparation." French Patent ONERA FR 2642080 (27/07/90).
27. M. Parlier and Ph. Colomban, "Composites a Matrice Ceramique Pour Applications Thermostructurales," *La Recherche Aerospatiale* **5-6**, 457-469 (1996).
28. D. D. Erikson, T. E. Wood and W. P. Wood, "Historical Development of Abrasive Grain," 100th Annual Meeting Am. Ceram. Soc., 3-6 may 1998, Cincinnati (USA), *Sol-Gel Processing Symposium, Ceramics Trans.* **95** (1998), Westerville (to be published).
29. H. G. Sowman, US Patents 3.795524, 3.709706, 3.793041, 3.916584, 4.047965, 4.125406
30. E. D. Whitney and P. N. Vaidyanathan, "Microstructural Engineering of Ceramic Cutting Tools," *Am. Ceram. Soc. Bull.* **67**(6), 1010-1014 (1988).
31. J. P. Mathers, T. E. Forester and W. P. Wood, "Sol-Gel Preparation of non-Oxide Abrasives," *Am. Ceram. Bull.* **68**(7), 1330-1335 (1989).
32. T. Hamasaki, K. Eguchi, Y. Koyanagi, A. Matsumoto, T. Utsunomiya and K. Koba, "Preparation and Characterization of Machinable Mica/Glass-Ceramics by the Sol-Gel Process," *J. Am. Ceram. Soc.* **71**, 1120-1124 (1988).
33. D. Qui, C. G. Pantano, "Sol-Gel Processing of Carbon Fiber-reinforced Glass Matrix Composites"; pp. 635-649, 3rd Int. Conf. on *Ultrastructure Processing of Ceramics, Glasses and Composites*, Edited by J. D. Mackenzie and D. R. Ulrich. J. Wiley & Sons, NY, 1987.
34. W. Pannhorst, M. Spallek, R. Brueckner, H. Hegaler, C. Reich, G. Grathwohl, B. Meier and D. S. Spelmann, "Fibre-reinforced Glass Ceramics fabricated by a novel Process," *Ceram. Eng. Sci. Proc.* **11**, 947-963 (1990).
35. R. S. Russell-Floyd, B. Harris, R. G. Cooke, J. Laurie, F. W. Hammett, R. W. Jones and T. Wang, "Application of Sol-Gel Processing Techniques for the Manufacture of Fiber-reinforced Ceramics," *J. Am. Ceram. Soc.* **76**(10), 2635-2643 (1993)
36. V. Guney, F. R. Jones, P. F. James and J. E. Bailey, "Ceramic Matrix Composites by Sol-Gel Processing," *Int. Phys. Conf. Ser* 111, IOP Publ. Ltd. 217-226 (1990).
37. M. Chen, F. R. Jones, P. F. James, J. E. Bailey, "Alumina Ceramic Matrices for Fibre Composites prepared by Modified Sol-Gel Processing," *Inst. Phys. Conf. Ser.* 111, IOP Publ. Ltd. 227-237 (1990).
38. J. Wu, M. Chen, F. R. Jones and P. F. James, "Mullite and Alumina-Silica Matrices for Composites by Modified Sol-Gel Processing," *J. Non-Cryst. Solids* **162**, 197-200 (1993).
39. J. Wu, F. R. Jones and P. F. James, "Mullite Matrix Fibre Reinforced Composites by Sol-Gel Processing," *Ceramics Trans.* **46**, *Adv. In Ceramic Matrix Composites II*, Westerville, 177-187 (1995).
40. J. Wu, M. Chen, F. R. Jones and P. F. James, "Characterization of Sol-Gel Derived Alumina-Silica Matrices for Continuous Fibre Reinforced Composites," *J. Eur. Ceram. Soc.* **16**, 619-626 (1996).
41. J. Jamet, D. Demange and J. Loubeau, "Procédé d'Elaboration de Composites," French Patent ONERA FR 2526785 (18-11-1985).
42. Ph. Colomban, M. Wey and M. Parlier, "Procédé d'Elaboration d'un Matériau Céramique par Infiltration d'un Précurseur Dans un Support Poreux Céramique," French Patent ONERA FR 2713222 (9-6-1995), European Patent 0656329 (17-6-1998).
43. M. Parlier and Ph. Colomban, "Near net-shape Matrix Sintering in 3D Fibre Reinforced CMC's using Hybrid Liquid Precursor-Powder Routes," Proc. ICCE/S, 5-11 july 1998, Las Vegas, D. Hui ed , 195-196.

44. J. L. Loubet, J. M. Georges, O. Marchesini and G. Meille, "Vickers Indentation Curves of Magnesium Oxide," *J. Tribology* **106**, 43-48 (1984).
45. I. A. Ashcroft, C. W. Laurence, T. D. Weihs and B. Derby, "In situ Measurement of the Elastic Moduli of Glass-Ceramic Thick Films," *J. Am. Ceram. Soc.* **75**(5), 1284-1286 (1992).
46. R. J. Kerans, R. S. Hay, J. Pagano and T. A. Parthasarathy, "The Role of the Fiber Matrix Interface in Ceramic Matrix Composites," *Am. Ceram. Soc. Bull.* **68**(2), 429-442 (1988).
47. R. Naslain, "Fiber-Matrix Interphases and Interfaces in Ceramic Matrix Composites Processed by CVI," *Compos. Interfaces* 1(3), 253-286 (1993).
48. C. Droillard, J. Lamon and X. Bourrat, "Strong Interfaces in CMC's. Conditions for Efficient Multilayered Interphases," *Mater. Res. Soc., Symposium Proc.* **365**, 371-376 (1995), MRS, Pittsburg.
49. R. S. Hay, M. D. Petry, K. A. Keller, M. K. Cinibulk and J. R. Welch, "Carbon and Oxide Coatings on Continuous Ceramic Fibres," *Mater. Res. Soc., Symposium Proc.* **365** (1995), MRS, Pittsburg.
50. J. J. Brennan, "Interfacial Studies of Fiber-reinforced Ceramic Composites"; pp. *269-289* in *High Temperature Ceramic Matrix Composites* Proc. HT-CMC1-6thEACM, R. Naslain, J. Lamon, D. Doumeingts, Woodheat Pub. Edited by, Abington Cambridge (UK), 1993.
51. C. H. Hsueh, "Interfacial Debonding and Pull-out Stresses of Fiber Reinforced Composites. VII. Improved Analysis for Bonded Interfaces," *Mater. Sci. Eng. A* **A154**, 125-137 (1992) and refs. therein.
52. D. B. Marshall, "Analysis of Fiber Debonding and Sliding Experiments in Brittle Matrix Composites," *Acta Metal. Mater.* **40**(3), 427-442 (1992).
53. C. Liang and J. W. Hutchinson, "Mechanics of the Fiber Push-out Test," *Mech. Mater.* **14**, 207-221 (1993).
54. F. Rebillat, J. Lamon, R. Naslain, E. Lara-Curzio, M. K Ferber and T. M. Besmann, "Interfacial Bond Strength in SiC/C/SiC Composite Materials as Studied by Single-Fiber Push-out Tests," *J. Am. Ceram. Soc.* **81**(4), 965-978 (1998).
55. T. P. Weiks and W. D. Nix, "Experimental Examination of the Push-down Technique for Measuring the Sliding Resistance of Silicon Carbide Fibers in a Ceramic Matrix," *J. Am. Ceram Soc.* **74**(3), 524-534 (1991).
56. O. Sudre, B. Passilly and M. Parlier, Microindentation of Ceramic Matrix Composites. Proc. 17th Ann. Conf. Composites and Adv. Ceramics, Coco Beach, Florida, 10-15 january 1993, *Ceram. Eng. Sci. Proc.* 180-187 (1994).
57. H. Mohrbacker, K. Van Acker, B. Blanpain, P. Van Houtte and J.P. Celis, "Comparative Measurement of Residual Stress in Diamond Coatings by low-incident-beam-angle-Diffraction and Micro-Raman Spectroscopy," *J. Mater. Res.* **11**(7), 1776-1782 (1996).
58. K. Kobayashi, Y. Inoue, T. Nishimura, M. Hirayama, Y. Akasaka, T. Kato and S. Ibuki, "Local-Oxidation-induced Stress Measured by Raman Microphobe Spectroscopy," *J. Electrochem. Soc.* **137**, 1987-0000 (1990).
59. I. de Wolf, J. Vanhellemont, A. Romano-Rodriguez, H. Norström and H. E. Maes, "Micro-Raman Study of Stress Distribution in local Isolation Structures and Correlation with Transmission Electron Microscopy," *J. Appl. Phys.* **71**(2), 898-906 (1992).
60. C. Galiotis, "Laser Raman Spectroscopy, a new Stress/strain Measurement Technique for the Remote and On-line Non-destructive Inspection of Fiber Reinforced Polymer Composites," *Materials Technology* **8**(9/10), 203-209 (1993).
61. R. J. Young, "Raman Spectroscopy and Mechanical Properties," in *Characterization of Solid Polymers*, S. J. Spells ed., 224-275, Chapman & Hall, London.
62. R. J. Young, "Analysis of Composites using Raman and Fluorescence Microscopy. A Review," *J. Microscopy* **185** (Part 2), 199-205 (1997),
63. G. Gouadec and Ph. Colomban, "Raman Extensometry, Anharmonicity and Stress," *Proc. JNC-11, Comptes Rendus des 11émes Journées Nationales sur les Composites, Arcachon, 18-20/11/98, J. Lamon and D. Baptisre eds., AMAC, Paris, 1998*, vol. II, 759-766.
64. F. Freund, "Highly ionic Hydroxides : unexpected Proton Conductivity in $Mg(OH)_2$ and Homologues"; pp. 138-157, in *Proton Conductors*, Edited by Ph. Colomban, Cambridge University Press, 1992.
65 M. Yoshikawa, G. Katagiri, H. Ishida, A. Ishitami and T. Akamatsu, "Resonant Raman Scattering of Diamond-like Amorphous Carbon Films," *Appl. Phys. Letts.* **52**(19), 1639-1641 (1988).
66. Y. G. Gogotsi, A. Kailer and K. G. Nichel, "Phase Transformations in Materials Studies by Micro-Raman Spectroscopy of Indentations," *Mat. Res. Innovat.* **1**, 3-9 (1997).
67. E. D. Miller, D. C. Nesting and J. V. Badding, "Quenchable Transparent Phase of Carbon," *Chem. Mater.* **9**(1), 18-22 (1997).
68. P. V. Huong, "Diamond and Diamond Films Studied by Raman Spectroscopy," *J. Mol. Struct.* **292**, 81-88 (1993).
69. Y. Sasaki, Y. Nishira, M. Sato and K. Okamura, "Raman Study of SiC Fibres Made from Polycarbosilane," *J. Mater. Sci.* **22**, 443-448 (1987).
70. R. Vidano and D. B. Rischbach, "New Lines in the Raman Spectra of Carbons and Graphite," *J. Am. Ceram. Soc.* **61**, 13-17 (1978).
71. H. Okamura, E. Sakuma, J. H. Lee, H. Mukaida, S. Misawa, K. Endo and S. Yoshido, "Raman Scattering of SiC: Application to the Identification of Heteroepitaxy of SiC Polytypes," *J. Appl. Phys.* **61**, 1134-1136 (1987).
72. J. N. Rouzaud, A. Oberlin and C. Benny-Bassez, "Carbon Films : Structure and Microtexture (Optical and Electron Microscopy, Raman Spectroscopy)," *Thin Solid Films* **105**, 75-96 (1983).
73. C. Laffon, A. M. Flanck, P. Lagarde, M. Laridjani, R. Hagege, P. Olry, J. Cotteret, J. Dixmier, J. C. Miquel, H. Hammel and A. P. Legrand, "Study of Nicalon®-based (Ceramic Fibres and Powders by EXAFS Spectrometry, X-ray) Diffractometry and some Additional Methods," *J. Mater. Sci.* **24**, 1503-1512 (1989).
74. G. Chollon, R. Pailler, R. Naslain and P. Olry, "Correlation between Microstructure and Mechanical Behaviour at High Temperature of a SiC Fibre with low Oxygen Content (Hi-Nicalon)," *J. Mater. Sci.* **32**, 1133-1147 (1997).

75. X. J. Ning and P. Pirouz, "The Microstructure of SCS-6 SiC fiber," *J. Mater. Res.* **6**(10), 2234-2248 (1991).
76. M. L. Sattler, J. H. Kinney, E. Zywicz, R. Alani and M. C. Nichols, "The Microstructures of SCS-6 and SCS-8 SiC Reinforcing Fibers," *Proc. 16th Ann. Conference and Exposition on Composites and Advanced Ceramics*, Cocoa Beach, January 7-10 (1992), Ceram. Trans., Westerville, Am. Ceram. Soc.
77. G. Gouadec, S. Karlin, J. Wu, M. Parlier, Ph. Colomban, "Chemical Physics and Mechanical Imaging of Ceramic Fibres Reinforced Ceramic or Metal Matrix Composites," Proc. JNC11, *Comptes Rendus des Onziémes Journées Nationales sur les Composites*, Arcachon, 18-20 nov. 1998, J. Lamon and D. Baptisre eds., AMAC, Paris (1998), vol. II, 617-625.
78. A. Vassel, "Interface Considerations in High-Temperature Titanium Metal Matrix Composites," *J. Microscopy* **185**, 303-309 (1997).
79. R. J. Young, D. Lu, R. J. Day, W. F. Knoff and H. A. Davis, "Relationship Between Structure and Mechanical Properties for Aramid Fibres," *J. Mater. Sci.* **27**, 5431-5440 (1992).
80. M. C. Andrews R. J. Young, "Analysis of the Deformation of Aramid Fibres and Composites using Raman Spectroscopy," *J. Raman Spect.* **24**, 539-544 (1993).
81. I. J. Beyerlein, M. S. Amer, L. S. Schadler and S. L. Phoenix, "New Methodology for Determining *in situ* Fiber, Matrix and Interface Sstresses in Damaged Multifiber Composites," *Sci. & Engin. of Composite Materials* (1998).
82. D. V. Bucci, M. J. Koczac and L. S. Schadler, "Micromechanical Investigations of Unidirectional C/C Composites via Micro-Raman Spectroscopy," *Carbon* **35**(2), 235-000 (1927).
83. X. Yang and R. J. Young, "Model Ceramic Fibre-reinforced Glass Composites Residual Thermal Stresses," *Composites* **25**(7), 488-493 (1994).
84. J. Wu and Ph. Colomban, "Raman Spectroscopic Study of the Stress Distribution in Continuous Fibre-reinforced CMC'." *J. Raman Spectr.* **28**, 523-529 (1997).